JOURNAL OF MATERIALS SCIENCE **38** (2003) 783–788

# Hackle or textured mirror? Analysis of surface perturbation in single crystal silicon

DOV SHERMAN
*Department of Materials Engineering, Technion-Israel Institute of Technology, Haifa 32000, Israel*
*E-mail: mtrdov@vmsa.technion.ac.il; dsherman@techunix.technion.ac.il*

The fracture surfaces of strip-like single crystal silicon specimens, loaded statically under three-point bending to fracture, revealed an exceptional behavior of surface perturbations generated during the unstably propagating crack. The observed perturbations presented a unique opportunity to study and interpret the relationship between the local crack tip velocity and the mirror and the hackle mechanisms. We show that the high amplitude, more disturbed perturbations are generated at low local crack front velocity, and therefore can termed as a mirror, while the lower amplitude, relatively smooth perturbations are associated with the fastest local crack front velocity, which is actually a hackle mechanism, in contrast to the current knowledge of crack velocity and the associated mirror and hackle mechanisms. 

## 1. Introduction

Universal routes of instabilities are accompanied a dynamically propagating crack in the following sequence: mirror, mist, hackle, and branching [1–5]. Mirror reflects a low velocity, low kinetic energy mechanism, with no or little surface perturbations. Mist is a surface perturbation of very low spatio-temporal amplitude that leads to the rougher hackle zone, formed at high velocity. If the unbalanced energy continues to grow, branching may take place, when the crack tip bifurcates in order to absorb the growing energy. These oscillations were not stable but rather grew in amplitude until branching occurred. The progressive damage mechanisms where extensively described by Frechette and coworkers [4, 5], and by Rice [3], especially for amorphous materials, but also by others for single crystals [6, 7].

In a previous work we have shown the unique perturbations generated in sapphire specimens having the same geometry and loading, and analyzed the profile of the perturbed crack front in one of the specimens, that revealed chaotic deterministic behavior [8–10]. Recent works, done in silicon by Hauch *et al.* [11] and Cramer *et al.* [12, 13], observed the steady movement of cracks with a high energy concentration on {111} and {110} cleavage planes. Perturbations parallel to the crack direction were observed in association with higher energy concentration. Velocity measurements of the crack tip in silicon and glass were performed [12, 13]. The relationship between crack tip velocity and the universal damage mechanisms was demonstrated [14].

The dynamic crack propagation in single crystal silicon, described in the current investigation provided a unique opportunity to further reveal the fundamental phenomena associated with unstable crack propagation in defect free single crystal brittle solids, especially the well known relationship between low-velocity, low-surface-perturbation and high-velocity, high-surface-perturbations. It is shown that the exact history of the crack propagation is required to distinguish among the different damage mechanisms.

## 2. Experimental program

### 2.1. Materials and specimens

Single crystal silicon, {001} type, 100 mm by diameter and 500 $\mu$m thick wafers where used in this investigation. The long-range order of these wafers, and the lack of point defects or dislocations enable exploration of the role of the only disturbance in the material, the cleavage planes.

The circular wafers were cut to strip-shaped specimens, each 10 mm wide, and inclined to the [110] direction by 3°. This angle is the cleavage plane inclination angle to the maximum $K_I$ plane at bending. This inclination is arbitrary, and yet provides more pronounced perturbations for the purpose of rigorous analysis. Branches may be developed in specimens with larger inclination angles. The final geometry of the specimens was of rectangular strips of 45 × 10 × 0.5 mm$^3$. Several specimens where tested, possessing practically the same behavior.

### 2.2. Experimental procedure

The loading configuration was of 3PB, as shown in Fig. 1. The specimens rested on a fully articulated 3PB fixture. The span was always 40 mm. The thickness/span ratio ensured that the maximum shear stress was less than 1 per cent of the maximum tensile stress ($\tau_{max}/\sigma_{max} = h/2L = 0.0063$).

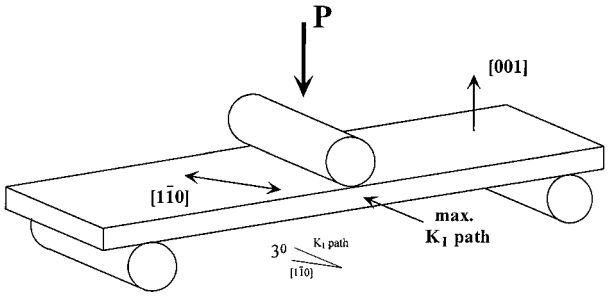


*Figure 1* Schematic of the geometry, loading, and relevant directions and planes.

The fracture surfaces of all the specimens were examined with optical microscope and a High Resolution Scanning Electron Microscope (HRSEM). The surface perturbation where scanned by Mahr Profilometer®, and by Atomic Force Microscope (AFM).

## 3. Results

No notch of pre-crack were introduced to the specimens in the current investigation, and therefore the strain energy stored in the material prior to cracking can be considered as high, which dictates the overall behavior of the surface perturbations. The broad understanding of the surface perturbations and their relations with the local crack front velocity must be followed by a comprehensive description of the damage evolution as the crack propagates into the material, the crack front velocity or relative velocity, and macroscopic and microscopic description of the perturbations. This chapter is therefore arranged by that order.

### 3.1. Crack path and crack profile

All the cracks initiated as a corner crack in one of the two corners that are subjected to high tensile stresses. The cracks in all the specimens propagated in a tortuous way for about 2 mm, Fig. 2a and b, resulting from the conflict between the maximum $K_I$ path (which is inclined to the [$\bar{1}\bar{1}$0] direction), the {111}, and the {110} cleavage planes. The crack then propagated, macroscopically, on an inclined plane with a measured angle of 35° to the [001] direction, which is, macroscopically, the {111} low energy cleavage plane, and demonstrating steady state surface perturbations for the vast length of the remaining cross section (over 6 mm in length), as shown in Fig. 2c. It is well understood [4, 10] that the tension/compression

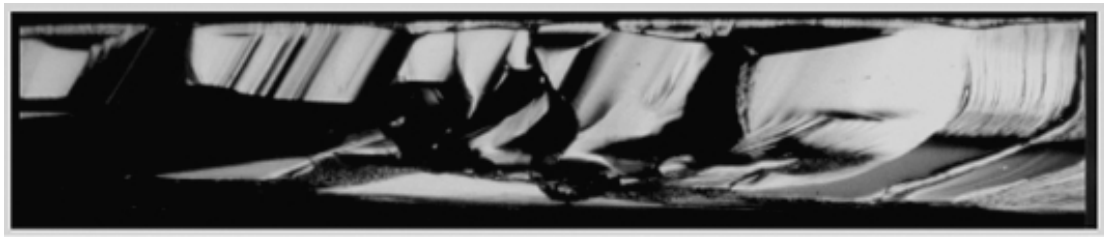

(a)

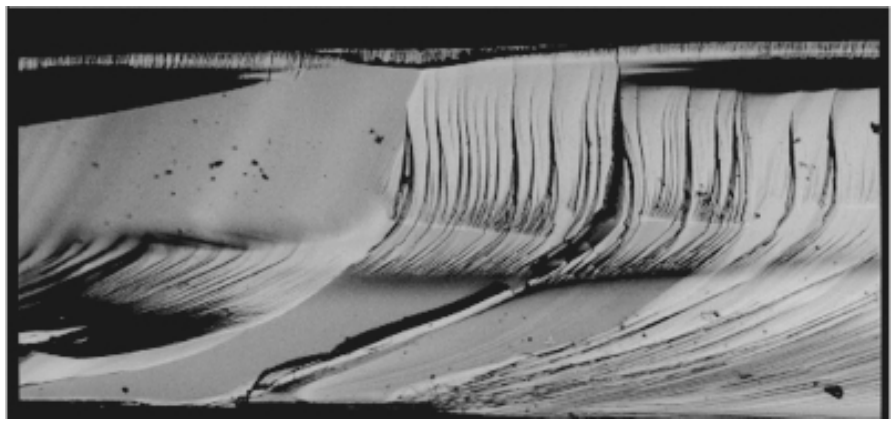

(b)

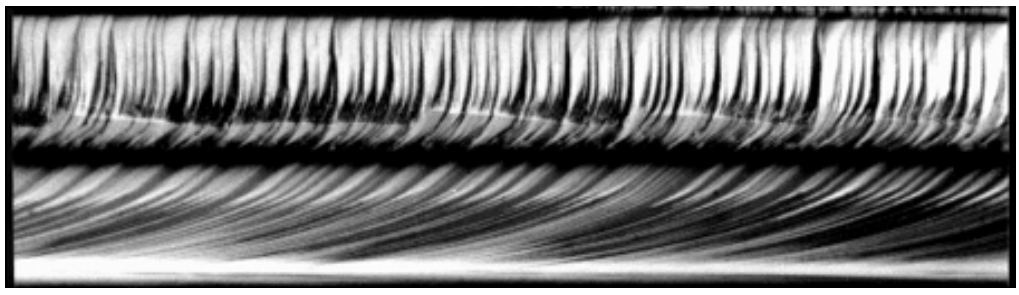

(c)

*Figure 2* Optical photograph of the fracture surface of the cracked silicon: the initial tortuous zone (a) magnification of the initiation of the surface perturbations (b), and the surface perturbations at steady state (c).

stresses, typical to bending, are the cause of the quarter elliptical nature of the crack front. Three major steps were identified in the current investigation for the crack propagation in the silicon specimens:

(i) After propagation in tortuous way (see above), the crack then advances on the {111} plane as a quarter elliptical, tensile crack in the lower portion of the beam, restrained by the upper portion, which is under compression, as schematically shown in Fig. 3a. As the constraint weakens, the 'tail' of the crack front penetrates into the upper portion of the specimens, previously under compression, Fig. 3b, forming a nearly straight crack front, inclined to the propagation direction by a shallow angle. The parallel crack velocity, $V_p$, in the $[1\bar{1}0]$ direction, is assumed constant at steady state, while the normal to the front velocity, $V_n$ is reduced sharply at the top surface (Fig. 3b).

(ii) The crack further advances such that the perturbations in the lower portion of the specimen are fully developed, those in the upper portion exposed at a velocity of $V_n$, which is nearly in the $[11\bar{2}]$ direction, the as shown in Fig. 3c.

(iii) At this stage, the perturbations at the beginning of the specimen are fully developed, as shown in Fig. 3d. The fracture surface of most of the specimen is constructed from perturbations at steady state, Fig. 3e (left). When the crack approaches the end of the specimen, the steady state no longer exists, Fig. 3e (right).

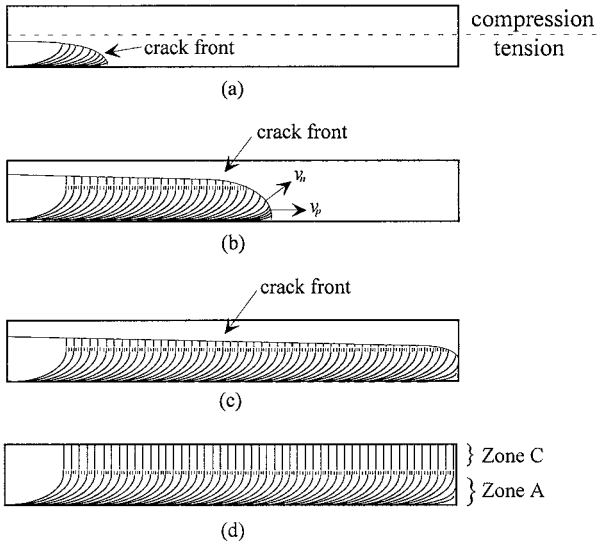


*Figure 3* Schematic presentation of the advancing crack in a silicon specimen. propagation as a quarter elliptical crack (a), hackle of the advancing crack (b), the crack approaching the edge of the specimen (c), changing the direction of crack's advance, and completion of the fracture mechanisms (d).

An important observation is the curved nature of the perturbations in silicon, compared to the faceted and straight nature of the perturbations in sapphire [8–10]. This behavior in sapphire is due to the interaction of the perturbations with secondary cleavage planes with small inclination to the primary crack plane. In the upper portion of the specimen, the path of the crack is that of a set of triangular saw tooth with angle of 150°, suggesting that the crack moves alternatively on $\langle 10\bar{1}0\rangle$ and $\langle 11\bar{2}0\rangle$ cleavage planes. Such secondary cleavage planes do not exist in silicon. Large, flat surfaces separated by a straight step generated by twisting mechanism constituted by crack movement on cleavage planes dictate the propagation in sapphire specimens in the lower portion of the cross section. These steps are curved in silicon specimens.

## 3.2. Analysis of the crack front and velocities

A higher magnification optical micrograph of the surface perturbations at steady state is shown in Fig. 4. The

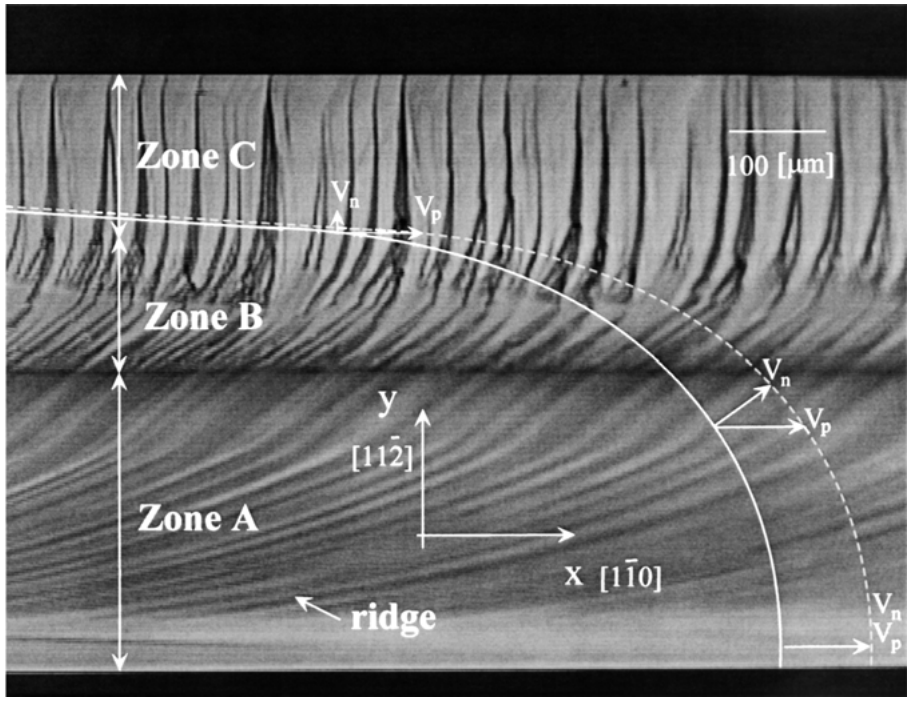


*Figure 4* The three zones of the surface perturbations and the plot of the crack front: elliptical in Zones A and B and linear in Zone C, and the typical velocities.

$x$, $y$, and $z$ axis in this scheme were chosen parallel to $[1\bar{1}0]$, $[11\bar{2}]$, and [111] directions, respectively, and $y = 0$ is set to be at the bottom of the specimen. The crack front at steady state of the dynamic crack propagation is of elliptical shape followed by a nearly straight line. At this stage, the crack front is advancing at a constant average velocity, $V_p$, in the $x$ direction. We distinguish among three zones of the crack profile. The instantaneous elliptical shape of the crack front in Zones A and B approximately obeys $y = b \cdot [1 - (x/a)^2]^{1/2}$, where $a$ and $b$ are the axes of the ellipse in the $x$ and $y$ directions. Their lengths are 515 and 453 $\mu$m, respectively (the height of the cross section is 612 $\mu$m). The ellipse is valid for $0 < y < 452$ $\mu$m. The last section of the crack front, namely the straight line, Zone C, is tangent to the ellipse, valid for $y > 452$ $\mu$m, and obeys $y = 612 - x/16$. An important observation seen clearly in Fig. 4 is that the perturbations form and evolve always *perpendicular* to the crack front. A single ridge is therefore initiated at the bottom surface of the specimen, where the velocity normal to the crack front, $V_n$, coincides with the parallel velocity, $V_p$. At this point the ridge's velocity is at its highest. It advances as a curved, step like perturbation and turns toward the center of the specimen, its velocity decreasing as the ridge approaches the end of Zone A (Fig. 4). The ridge enters the transient Zone B, where the velocity vector slows down significantly. In zone C, the velocity vector is almost normal to the surface of the specimen, which now has the shape of a straight line. The amplitude of the normal velocity vector in this zone is small. A single ridge, which is initiated at the bottom surface of the specimen, is therefore making almost a 90° change in direction. An important observation is that not only does the ridge not advance on the low energy cleavage plane, it also changes its direction, in a relatively smooth manner. The observations of the crack perturbations suggest that the cleavage planes have only a minor role in the development of the perturbations (see below).

The relative velocity $V_n/V_p$, shown in Fig. 5, was obtained by computing the normal to the function describing the crack profile. The normal velocity in Zone C is only about 6% of the parallel velocity. The derivative of $V_n/V_p$ with respect to the Y axis (Fig. 5) explores the bounds between the different zones; Zone A is characterizes by a linear $\mathrm{d}(V_n/V_p)/\mathrm{d}y$, while Zone C by a constant normal velocity, $V_n$. The transition zone, Zone B, is characterized by rapid changes of this derivative. It is noted that the maximal terminal velocity of unconstrained Mode I crack in single crystal silicon on {111} plane was measured as 3500 m/sec [13]. Assuming $V_p$ coincides with this terminal velocity, $V_n$ in Zone C is only 210 M/sec.

### 3.3. Description of the surface perturbations

The fracture surface the specimens were scanned with a Mahr© Perthometer along ten lines at the zone of steady state perturbations, each of which is parallel to the specimen surface. The length of each scan was nominally 4 mm, and the distance between the scanned lines was an average of 50 $\mu$m. The profiles were scanned with a diamond stylus of a 2 $\mu$m diameter. The horizontal resolution was 0.2 $\mu$m for the A and B type perturbations and 0.1 $\mu$m for the C perturbations. The vertical resolution is 10 nm nominally. Typical profiles in the A, B, and C regions are shown in Figs 6a to c, respectively, where the overall length scale in these figures is 1500 $\mu$m. The step-like Zone A perturbations have a spatial frequency varying between 30 to 100 $\mu$m, the jumps from step to step is about 0.2 $\mu$m, and there are second order perturbations of smaller amplitude, superimposed on the primary perturbations. The Zone C

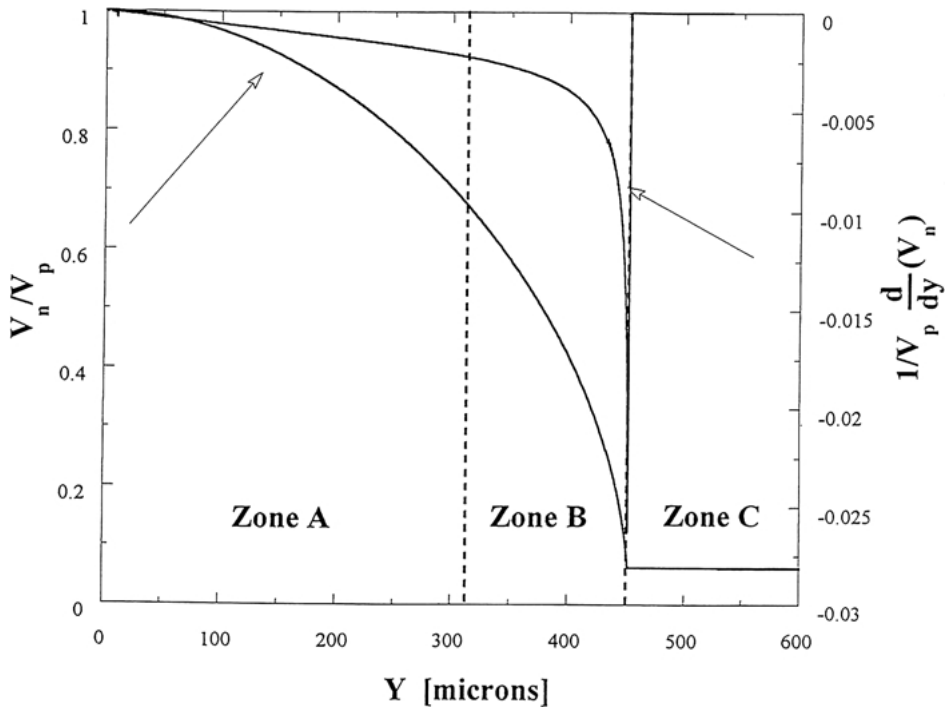


*Figure 5* The normalized velocity, $V_n/V_P$, and its derivative with respect to the $Y$ axis as a function of the $Y$ axis.

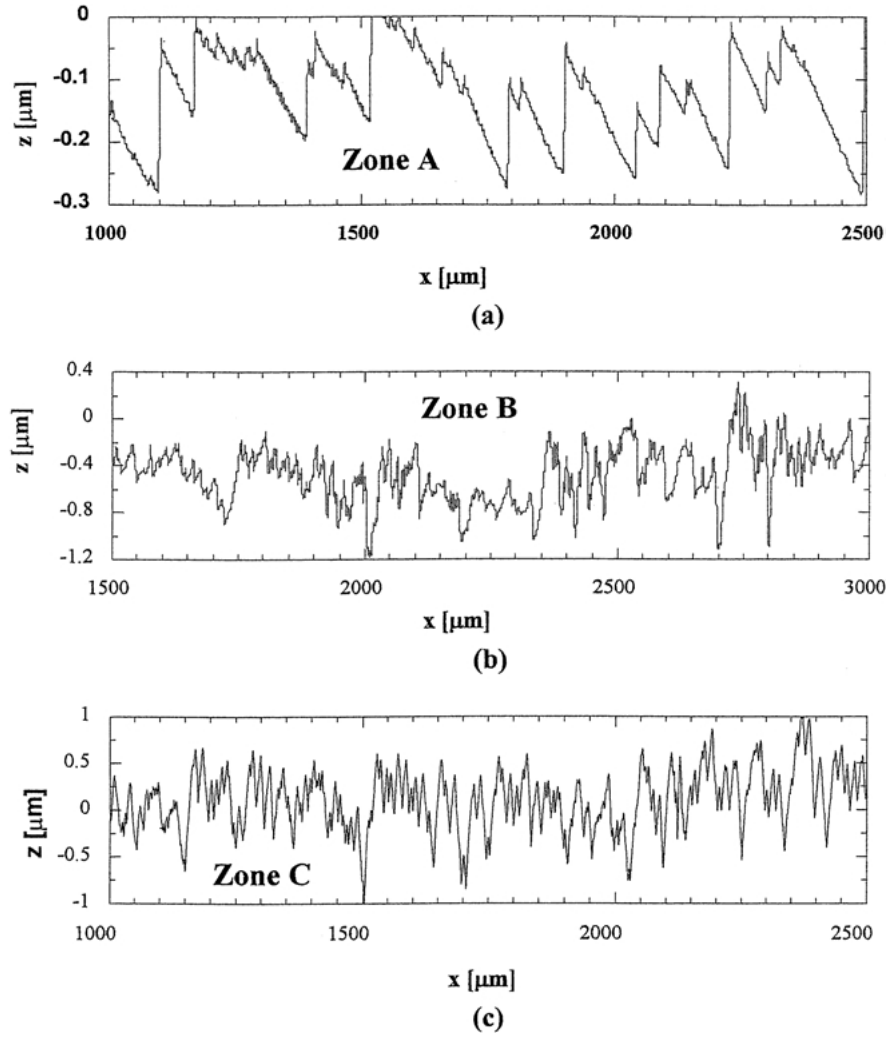


*Figure 6* Surface perturbations along three lines, typical of each zone: (a) and Zone A, (b) Zone B, and (c) Zone C.

perturbations have average amplitude of 1 $\mu$m and a frequency of about 30 $\mu$m.

The surface of typical step-like ridges, Zone A, having the higher normal velocity were depicted with an Atomic Force Microscope (AFM), as shown in Fig. 7a. An AFM photograph of the surface perturbations in Zone C is shown in Fig. 7b. These perturbations are associated with the smallest normal velocity, $V_n$, and have the highest amplitude. While the perturbations seem to be made of distinctive facets, the areas of transition between the facets are blunt, and the facets themselves are not flat and smooth as expected from cleavage surfaces.

## 4. Discussion

Based on the experimental measurements and observations, the following is concluded:

(i) While macroscopically the crack is propagating on the preferred (111) low energy cleavage plane, a more rigorous surface analysis demonstrated a very complicated crack path, so that, locally, the crack propagates on a non-preferred cleavage plane, and maneuvers itself smoothly along various planes. This is evident from the macroscopic curvatures of the ridges of zone A and the surface morphology of the perturbations in Zone C. We attribute this behavior to the nearly isotropic behavior of the fracture energy of the cleavage planes in silicon.

(ii) The same perturbations have been observed by the authors in single crystal sapphire [8–10] and lately in single crystal $Li_2NiO_3$ (although their crystal structure is different from that of silicon), which constitute them as universal fracture mechanisms under the described conditions.

(iii) The three distinct zones are defined by the changes in the normal velocity along the crack front, namely, surface perturbations are very sensitive to changes in normal velocity.

(iv) The surface perturbations are perpendicular to the propagating crack front, and with the same rational, their propagation velocity coincides with the normal velocity.

(v) While the perturbations in zone A may be identified as a hackle mechanism, typical to high velocity, unstable crack propagation, the perturbations in Zone C are presumably mirror, as the crack velocity is low, and this is therefore termed *'Textured Mirror'*. The reason for the perturbed mirror mechanisms is the 'roughness' generated by the transition Zone B. Furthermore, while it is known that mirror mechanisms are characterized by very small surface perturbations, it was shown in this

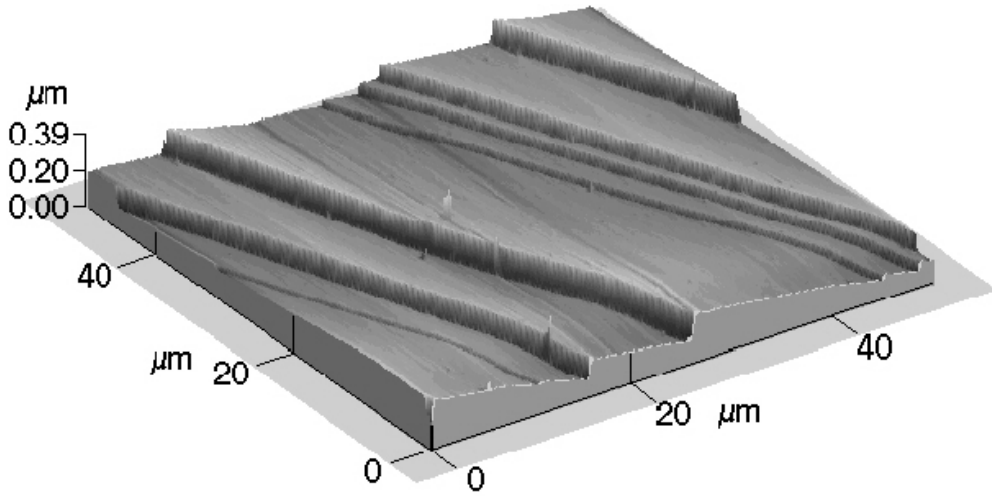


(a)

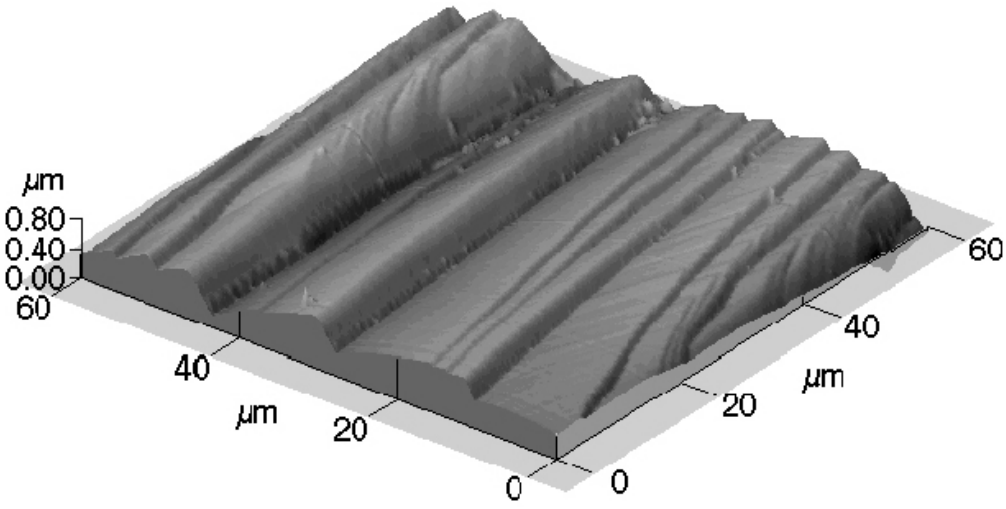


(b)

*Figure 7* AFM simulations of the perturbations in Zone A (a), and in Zone C (b).

investigation that mirror mechanisms may have large amplitude perturbations.

## 5. Summary

The combination of defect-free single crystal silicon specimens fractured under three point bending in the configuration described above, the uniqueness of the crack profile having a varying normal crack velocity along the crack profile, enabled the investigation of unique surface perturbations, and to reach several fundamental conclusions regarding the basic fracture mechanisms, mirror and hackle, resulting from dynamical instabilities. It was shown that the classical analysis, that relates mirror mechanisms to low velocity and low, almost vanishing, perturbation, and, on the other hand, hackle mechanism to high velocity and high amplitude of surface perturbations is incorrect in the current loading configuration. Therefore, any conclusion regarding fundamental fracture mechanisms should be based on a rigorous analysis and knowledge of the history of the formation of the fracture surface perturbations.

## References

1. L. B. FREUND, "Dynamic Fracture Mechanics" (Cambridge University Press, Cambridge, 1990).
2. B. LAWN, "Fracture of Brittle Solids" 2nd ed., Cambridge Solid State Science Series (Cambridge, 1993).
3. R. W. RICE, in "Advances in Ceramics," Vol. 22 (1986) p. 3.
4. V. D. FRECHETTE, "Failure Analysis of Brittle Materials," Advances in Ceramics, Vol. 28 (1990).
5. T. A. MICHALSKE, M. SINGH and V. D. FRECHETTE, ASTM STP 745, edited by W. Freiman and E. R. Fuller (ASTM, Philadelphia, PA, 1980) p. 3.
6. A. BALL and B. W. PAYNE, *J. Mater. Sci.* **11** (1976) 731.
7. S. M. WIEDERHORN, *J. Amer. Ceram. Soc.* **52** (1969) 485.
8. D. SHERMAN and I. BE'ERY, *Phys. Rev. Lett.* **80** (1998) 540.
9. *Idem.*, *Physica* D **119** (1998) 424.
10. *Idem.*, *J. Mater. Sci.* **35** (2000) 1283.
11. J. A. HAUCH, D. HOLLAND, M. P. MARDER and H. L. SWINNEY, *Phys. Rev. Lett.* **82** (1999) 3823.
12. T. CRAMER, A. WANNER and P. GUMBSCH, *ibid.* **85** (2000) 788.
13. *Idem.*, *Zeitschrift-fur-Metallkunde* **90** (1999) 675.
14. J. FINEBERG, S. P. GROSS, M. MARDER and H. L. SWINNEY, *Phys. Rev.* B **45** (1992) 5146.

*Received 30 January*
*and accepted 24 September 2002*